# Analysis of an Orbiting Three-Rigid-Body System's Dynamics

Daniele Pagnozzi[†,*] and James D. Biggs[**,*]

[*] *Department of Mechanical & Aerospace Engineering University of Strathclyde, Glasgow, Scotland, UK*
[†] *daniele.pagnozzi@strath.ac.uk*
[**] *james.biggs@strath.ac.uk*

**Abstract.** The development of multi-joint-spacecraft mission concepts calls for a deeper understanding of their nonlinear dynamics to inform and enhance system design. This paper presents a study of a three-finite-shape rigid-body system under the action of an ideal central gravitational field. The aim is to gain an insight into the natural dynamics. The Hamiltonian dynamics is derived and used to identify relative attitude equilibria of the system with respect to the orbital reference frame. Then a numerical investigation of the behaviour far from the equilibria is provided using tools from modern dynamical systems theory such as energy methods, phase portraits and Poincarè maps. Results reveal a complex structure of the configuration manifold underlying the dynamics as well as the existence of connections between some of the equilibria. Stable equilibrium configurations appear to be surrounded by very narrow regions of regular and quasi-regular motions. Trajectories evolve on chaotic motions in the rest of the domain.

**Keywords:** Space Multi-body System, Rigid Body Dynamics, Hamiltonian Mechanics, Nonlinear Systems Analysis, Poincaré Map
**PACS:** 02.30.Hq, 02.40.Vh, 02.40.Yy, 05.45.Pq, 45.20.Jj, 45.50.Jf

## INTRODUCTION

Emerging mission concepts involve the use of multi-joint-satellite systems. These can be categorised into two main areas of application: on-orbit satellite servicing and active debris removal. Many mission concepts, see [1], [2], require two main bodies connected via hinges, robotic arms or tethers. For instance, the German Aerospace Centre DLR mission Deutsche Orbitale Servicing Mission (DEOS), [3, 4], and the Orbital Express Demonstration System (OEDS) flight test, [5, 6]. DEOS is a semi-autonomous satellite endowed with a robotic arm. Its mission is to berth, secure and de-orbit malfunctioned satellites from low earth orbit. The OEDS flight test, flown from March to July 2007, was a mission to demonstrate the required capabilities to autonomously service satellites on-orbit in different scenarios. Both these examples fall within the category of space multi-body systems. In particular, they may be modeled as a three-body system after the grasping/docking phase of the mission, where the two main bodies are connected together via a rigid link.

According to the definition in [7], a multi-body system is defined to be a collection of subsystems, called bodies, kinematically constrained which may undergo large translations and rotational displacements. This definition captures both space and terrestrial systems. Space systems differ from terrestrial systems in that they are not subject to a uniform gravity force[1] and do not have an anchorage pivot.

In mechanics, space multi-body problems are generally non-integrable as they are high dimensional systems with only two conserved quantities (when non-conservative forces are excluded): the total mechanical energy and the total angular momentum. These systems have a highly complex nature, characterised by their nonlinear dynamics, with interdependent orbital and attitude dynamics. All this makes the behaviour difficult to predict and so it is important that research into their global dynamics is undertaken. Understanding the underlying dynamics of the system can aid efficient system and control design. This is important because, in space, energy demands and actuator constraints are critical factors (for instance, reductions in fuel and power usage directly influences the useful operative life of the spacecraft, the weight and the mission costs). Dubowsky and Papadopoulos, who studied extensively free-flying and free-floating robotic systems, examples of space multi-body systems, suggest that understanding their fundamental dynamic behaviour will improve system design, [8], and that it will aid the development of solutions to problems of

[1] Constant in direction and magnitude.

planning and control, [9] and [10]. In addition, as achieved in orbital dynamics, see [11], and more recently in attitude dynamics [12, 13], understanding the natural motions of the system offers the possibility to exploit them to design fuel efficient motions (when the time scale of the natural motions is comparable with the missions' operational timescale).

The aim of this paper is to study the dynamics of a multi-body space system made of three finite-shape rigid-bodies joined by ideal hinges. The system is assumed to be under the action of an ideal central gravity field only. As a consequence, when all the initial conditions lie on a plane, the system's motion can be proved to evolve on a plane, [14]. The problem is, therefore, restricted to the planar case. As a further assumption, the characteristic dimensions of the bodies are assumed to be negligible relative to the central body, as a spacecraft orbits a much larger celestial body. The novelty of this work is in using finite-shape bodies to model the problem in order to have a more accurate description of the system. Moreover, the methods of analysis applied to study a multi-spacecraft problem are relatively new in this field.

The content of the paper is as follows:

- In Section 2 the three-body model is introduced. The corresponding Hamiltonian dynamics for the multi-body system in orbit around a large celestial body is derived.
- In Section 3 relative equilibria are identified, approximations are introduced to uncouple the orbital dynamics from the attitude dynamics and an analysis of the Hamiltonian of the attitude dynamics is addressed numerically via Hamiltonian plots.
- In Section 4 the behaviour far from the equilibria is investigated using numerical tools, such as phase portraits and a Poincaré map.
- In Section 5 results are discussed. They are compared with the ones from a two-rigid-body system and their implications for future multi-body space system design and control are discussed.

## THE PHYSICAL MODEL

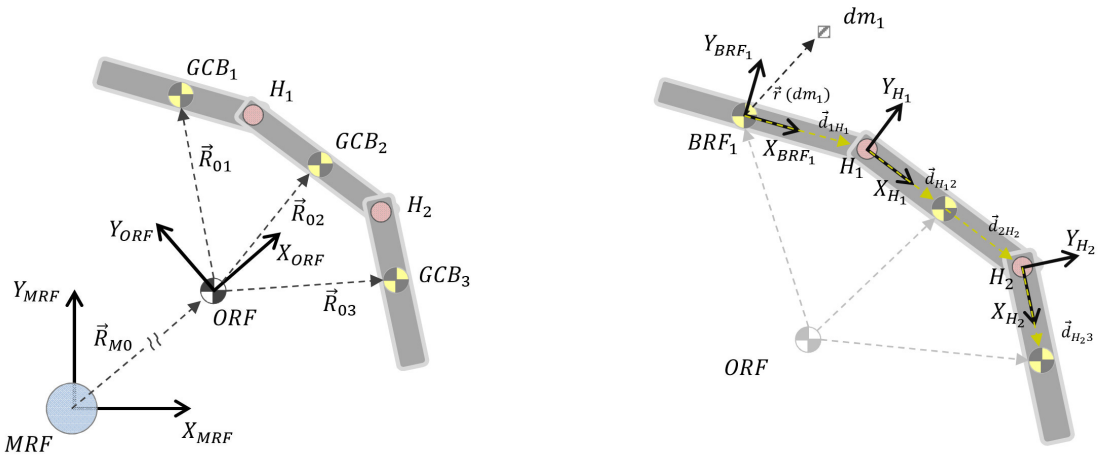


1: Illustrations of the system and of the vector set used to describe it

In this paper we take inspiration from [15], [16], [10], and [17] to derive the Hamiltonian equations of motion. This form is convenient to analyse the equilibria and their non-linear stability.

The following reference frames are used:

1. Main Reference Frame
2. Orbital Reference Frame
3. Body Reference Frame (one per body)

The Main Reference Frame (*MRF*) is assumed to be inertial and fixed in space; its origin is the origin of the gravity field. The $X|_{MRF}$ and $Y|_{MRF}$ plane is assumed to be the orbital plane with the $z-axis$ parallel to the orbital angular momentum vector.

The Orbital Frame (*ORF*) is not inertial; its origin is the instantaneous overall center of mass of the multi-body system. Its $x-axis$ is parallel to the position vector of the origin w.r.t. the *MRF*; the z-axis is taken as parallel to the $Z|_{MRF}$ and consequently the y-axis will be parallel to the local horizon such that it forms a right handed frame.

Every single body will be given its own reference frame ($BRF_i$ - where the subscript $i$ is a number identifying the body), with the origin its center of mass and orientation set according to the principal axes of inertia.

## System configuration variables

A particle mass of the $i$-th body is described by the following position vector:

$$\begin{aligned}\vec{R}(\delta m) = \quad & \vec{R_{M0}} + \vec{R}_{0i} + \vec{r}_i(\delta m) = \\ & \vec{R_{M0}} + \mathbf{T}_{M0}\left(\{\vec{R}_{0i}\}_0 + \mathbf{T}_{0i}\left\{\vec{r}_i(\delta m)\right\}_i\right)\end{aligned} \tag{1}$$

The following notation has been adopted: $\vec{R_{M0}}$ position vector of the overall center of mass w.r.t. the *MRF* ; $\vec{R}_{0i}$ is the position vector of the i-th body center of mass w.r.t. the *ORF* ; $\vec{r}_i(\delta m)$ is the position vector of the infinitesimal mass $\delta m$ w.r.t. the $BRF_i$; $\mathbf{T}_{AB}$ is a coordinate transformation matrix which rotates a generic vector from reference frame A to the reference frame B. In particular the subscripts: M refers to the *MRF*; 0 refers to the *ORF* and $i$ refers to the i-th *BRF*.

Note that $\mathbf{T}_{M0}$ depends on the orbital true anomaly $\nu$ only and $\mathbf{T}_{0i}$ depends on the attitude angle of the i-th body $\theta_i$ only, as the problem is set as 2-D.
Moreover: $\mathbf{T}_{Mi} = \mathbf{T}_{M0}\mathbf{T}_{0i}$. Also, note that the position vector of the *ORF* can be described in polar coordinates as $\vec{R}_{M0} = \mathbf{T}_{M0}\{R_0, 0\}$. Three constraint equations are introduced:

$$m_1\vec{R}_{01} + m_2\vec{R}_{02} + m_3\vec{R}_{03} = \vec{\mathbf{0}} \quad ; \quad \vec{R}_{01} + \vec{d}_{1H_1} + \vec{d}_{H_1 2} = \vec{R}_{02} \quad ; \quad \vec{R}_{02} + \vec{d}_{2H_2} + \vec{d}_{H_2 3} = \vec{R}_{03} \tag{2}$$

Where $\vec{d}_{1H_1}$, $\vec{d}_{H_1 2}$, $\vec{d}_{2H_2}$ and $\vec{d}_{H_2 3}$ are the position vectors of the hinges with respect to the bodies centers of mass and $\vec{\mathbf{0}}$ is the null vector. As the bodies are assumed to be rigid, the vectors are fixed in their respective body reference frames. The first identity is satisfied because it has been set the overall center of mass of the system as origin of the *ORF*. The second and third identities describe that the bodies are joined at the hinges via rotational joints.

Using the constraints to reduce the system, this is fully described by the following set of configuration variables:

$$\{R, \nu, \theta_1, \theta_2, \theta_3\} \quad ; \quad \left\{\dot{R}, \dot{\nu}, \dot{\theta}_1, \dot{\theta}_2, \dot{\theta}_3\right\} \tag{3}$$

where $R$ is the modulus of the orbital vector; $\nu$ is the orbital anomaly angle; $\theta_1, \theta_2, \theta_3$ are the attitude angles of the bodies which describe the inclination of the $X|_{BRF_i}$ axis with respect to the $X|_{ORF}$ axis.

## Kinetic Energy

Differentiating eq. (1) with respect to time, using the reduced variables set and applying the inner product yields the kinetic energy of the $i$-th body as:

$$\mathscr{K}_i = \frac{1}{2}\int_{\mathscr{B}i} < \dot{\vec{R}}(\delta m), \dot{\vec{R}}(\delta m) > \delta m \tag{4}$$

Note that the rotation matrices satisfy the differential equation $\frac{d\mathbf{T}_{AB}(\psi)}{dt} = \mathbf{T}_{AB}\Omega_{AB}$ with $\Omega_{AB}$ a skew-symmetric matrix function of $\frac{d\psi}{dt} = \omega_{AB}$ only. After some algebra eq (4) becomes:

$$\begin{aligned}\mathscr{K} = & \frac{m}{2}(\dot{R}^2 + R^2\omega_{M0}^2) + \lambda_{12}(\omega_{01} + \omega_{M0})(\omega_{02} + \omega_{M0})c_{\theta_1-\theta_2} + \\ & \lambda_{13}(\omega_{03} + \omega_{M0})(\omega_{01} + \omega_{M0})c_{\theta_1-\theta_3} + \lambda_{23}(\omega_{03} + \omega_{M0})(\omega_{02} + \omega_{M0})c_{\theta_2-\theta_3} + \\ & \frac{1}{2}\hat{I}_1(\omega_{01} + \omega_{M0})^2 + \frac{1}{2}\hat{I}_2(\omega_{02} + \omega_{M0})^2 + \frac{1}{2}\hat{I}_3(\omega_{03} + \omega_{M0})^2\end{aligned} \tag{5}$$

Where: $m = m_1 + m_2 + m_3$ total mass of the system; $\|\dot{\vec{R}}\|^2 = \dot{R}^2 + R^2\Omega_{M0}^2$ is the term related with the translational kinetic energy of the $ORF$ ; $\varepsilon_{ij} = (m_i m_j)/m$ ; $\lambda_{12} = d_{1H_1}[d_{2H_2}\varepsilon_{13} + d_{H_1 2}(\varepsilon_{12} + \varepsilon_{13})]$; $\lambda_{13} = d_1 d_{H_2 3}\varepsilon_{13}$ ; $\lambda_{23} = d_{H_2 3}[d_{H_1 2}\varepsilon_{13} + d_{2H_2}(\varepsilon_{13} + \varepsilon_{23})]$; $\hat{I}_1 = I_1 + d_{1H_1}^2(\varepsilon_{12} + \varepsilon_{13})$ ; $\hat{I}_2 = I_2 + d_{H_1 2}^2\varepsilon_{12} + d_{2H_2}^2\varepsilon_{23} + \varepsilon_{13}(d_{H_1 2} + d_{2H_2})^2$; $\hat{I}_3 = I_3 + d_3^2(\varepsilon_{13} + \varepsilon_{23})$; $c_{\theta_i - \theta_j} = cos(\theta_i - \theta_j)$. Note that $\hat{I}_i$ is the augmented inertia of the body. Moreover it has been assumed that the bodies' centers of mass are aligned with the hinges and the generic position vector of the hinge takes the form $\{\vec{d}_{ij}\}_i = (d_{ij}, 0)$ in its body reference frame.

## Potential Energy

The effect of gravity on every single body is considered. This depends on the shapes and the attitudes of the bodies. In order to obtain a simple form of the potential functions, these are expanded in Taylor series and only the terms up to the third degree will be considered. The bodies are assumed to have a characteristic length negligible compared with the orbital radius, have a quasi 1-D shape and constant density. The derivation of the approximated form of the potential is inspired by a well known procedure, see for instance [18] or [19], and it is described in detail in [20]. The final form of the potential energy is as follows:

$$\begin{aligned}\mathscr{U} =& \mathscr{U}_1 + \mathscr{U}_2 + \mathscr{U}_3 = \\ & -\mu\frac{m}{R} + -mu\frac{1}{4R^3}\{\hat{I}_1 + \hat{I}_2 + \hat{I}_3 - [-3\hat{I}_1 c_{2\theta 3} - 3\hat{I}_2 c_{2\theta 4} - 3\hat{I}_3 c_{2\theta 5} + \\ & -8\lambda_{12}c_3c_4 - 8(\lambda_{13}c_3 + \lambda_{23}c_4)c_5 + 4\lambda_{12}s_3s_4 + 4(\lambda_{13}s_3 + \lambda_{23}s_4)s_5]\};\end{aligned} \tag{6}$$

Again the trigonometric functions have been shortened using the notation: $cos(\phi) = c_\phi$ and $sin(\phi) = s_\phi$.

## HAMILTONIAN DYNAMICS

Let the name of the variables be changed to the following, in order to coincide with the general Lagrangian notation:

$$\{R_0, \nu, \theta_1, \theta_2, \theta_3\} \quad \equiv \quad \{q_1, q_2, q_3, q_4, q_5\} \tag{7}$$

By constructing the Lagrangian function of the system $\mathscr{L} = \mathscr{K} - \mathscr{U}$ and applying the Legendre transform, momenta follow in the form:

$$\vec{p} = \mathbf{J}\,\dot{\vec{q}} \tag{8}$$

with

$$\mathbf{J} = \begin{bmatrix} m & 0 & 0 & 0 & 0 \\ 0 & J_{2,2} & \hat{I}_1 + c_{12}\lambda_{12} + c_{13}\lambda_{13} & \hat{I}_2 + c_{12}\lambda_{12} + c_{23}\lambda_{23} & \hat{I}_3 + c_{13}\lambda_{13} + c_{23}\lambda_{23} \\ 0 & \hat{I}_1 + c_{12}\lambda_{12} + c_{13}\lambda_{13} & \hat{I}_1 & c_{12}\lambda_{12} & c_{13}\lambda_{13} \\ 0 & \hat{I}_2 + c_{12}\lambda_{12} + c_{23}\lambda_{23} & c_{12}\lambda_{12} & \hat{I}_2 & c_{23}\lambda_{23} \\ 0 & \hat{I}_3 + c_{13}\lambda_{13} + c_{23}\lambda_{23} & c_{13}\lambda_{13} & c_{23}\lambda_{23} & \hat{I}_3 \end{bmatrix} \tag{9}$$

where $J_{2,2} = mq_1^2 + \hat{I}_1 + \hat{I}_2 + \hat{I}_3 + 2(c_{12}\lambda_{12} + c_{13}\lambda_{13} + \lambda_{23}c_{23})$. The Hamiltonian function follows as:

$$\mathscr{H} = \mathscr{K}(\vec{q}, \vec{p}) + \mathscr{U}(\vec{q}) = \frac{1}{2}\vec{p}^{Tr}\mathbf{J}(\vec{q})^{-1}\vec{p} + \mathscr{U}(\vec{q}) \tag{10}$$

Thereafter, the Hamilton's equations are:

$$\frac{\partial\mathscr{H}}{\partial\vec{p}} = \mathbf{J}^{-1}\vec{p} \qquad ; \qquad \frac{\partial\mathscr{H}}{\partial\vec{q}} = \frac{1}{2}\vec{p}^{Tr}\frac{\partial\mathbf{J}^{-1}}{\partial\vec{q}}\vec{p} + \frac{\partial\mathscr{U}(\vec{q})}{\partial\vec{q}} \tag{11}$$

Because of the absence of dissipative forces, the total mechanical energy and total angular momentum are conserved (the variable $q_2$ is cyclic). However, a continuous exchange of energy and angular momentum between the two bodies and between orbital and attitude dynamics take place. The Hamiltonian can be split in two contributions:

$$\mathscr{H} = \mathscr{H}_{Att} + \mathscr{H}_{Orb} \tag{12}$$

$\mathscr{H}_{Att}$ depends on all the variables but $q_2$; the $\mathscr{H}_{Orb}$ is function of the orbital elements only. Their order of magnitude are significantly different: $o(\mathscr{H}_{Att}) \ll o(\mathscr{H}_{Orb})$. As a consequence, the orbital dynamics can be uncoupled by the attitude dynamics introducing an approximation error between exact orbital motion and approximated one that can be proved to be of the order of centimeters for systems orbiting the Earth, [20]. This allows us to focus on the attitude dynamics only.

## Equilibria

The relative equilibria of the attitude dynamics, i.e. equilibria of the system with respect to the *ORF*, are defined by: $\{\dot{q}_3\,,\dot{q}_4\,,\dot{q}_5\,,\dot{p}_3\,,\dot{p}_4\,,\dot{p}_5\} = \vec{\mathbf{0}}$. This set of equations has a solution for circular orbits only and at the following configurations:

$$\left(\kappa\,\pi\,,\ \kappa'\,\pi,\ \kappa''\,\pi\right) \qquad \text{and} \qquad \left(\tau\,\frac{\pi}{2}\,,\ \tau'\,\frac{\pi}{2}, \tau''\,\frac{\pi}{2}\right) \qquad \text{with} \qquad \kappa\,,\,\kappa'\,,\,\kappa'' \in \mathbb{Z} \qquad \tau\,,\,\tau'\,,\,\tau'' \in \mathbb{Z}_0 \tag{13}$$

This defines a number of 42 equilibria over the domain $S \times S \times S$, which can be grouped in six different classes depending on the symmetries of the configurations.

## Hamiltonian Maps

Let the attitude Hamiltonian, for given initial conditions, be defined by:

$$\mathscr{H}_{Att}|_{t=0} = \mathscr{H}_{Att} : \{\vec{q}_0, \vec{p}_0\} \equiv \left\{\vec{q}_0, \mathbf{J}(\vec{q}_0)\,\vec{\dot{q}}_0\right\} \quad \text{with} \quad \vec{q}_0 = \{q_{10}, ..., q_{50}\}\ ;\ \vec{\dot{q}}_0 = \{\dot{q}_{10}, ..., \dot{q}_{50}\} \tag{14}$$

Then, let be defined the following function of the bodies'attitude angles:

$$\tilde{\mathscr{H}}_{Att} = \tilde{\mathscr{H}}_{Att}(q_{30}, q_{40}, q_{50}) \equiv \mathscr{H}_{Att}|_{t=0} :\ \{\dot{q}_{30}, \dot{q}_{40}, \dot{q}_{50}\} = \vec{0} \quad \text{with} \quad (q_{30}, q_{40}, q_{50}) \in S \times S \times S \tag{15}$$

This function will provide the energy state associated with each motion starting from the point $(q_{30},\, q_{40},\, q_{50})$ with zero bodies' initial spinning rates. For *circular orbits* (where relative attitude equilibria exist):

$$\begin{aligned} q_1 \simeq const\ ,\ p_1 \simeq const\ ,\ p_2 \simeq const \Rightarrow & \mathscr{H} = \mathscr{H}(q_3, q_4, q_5, p_3, p_4, p_5) \\ & \text{or equivalently} \mathscr{H} = \mathscr{H}(q_3, q_4, q_5, \dot{q}_3, \dot{q}_4, \dot{q}_5) \end{aligned} \tag{16}$$

Hence, in this case, given $(q_3(t), q_4(t), q_5(t), \dot{q}_3(t), \dot{q}_4(t), \dot{q}_5(t)) = (q_{30}, q_{40}, q_{50}, 0, 0, 0)$ for $t = 0$:

$$\tilde{\mathscr{H}}_{Att}(q_3(t), q_4(t), q_5(t)) \leq \tilde{\mathscr{H}}_{Att}(q_{30}, q_{40}, q_{50}) \tag{17}$$

as a consequence that for null spinning rates the value of the kinetic energy is at its minimum and the total mechanical energy must be constant.

A representation of the function $\tilde{\mathscr{H}}_{Att}(q_{30}, q_{40}, q_{50})$ is provided for a system on a circular orbit with a nominal altitude of 300 km above the Earth in the case of three equal bodies with the parameters listed in table 1. This set of parameters has been chosen according to the work in [20], where symmetry was noted to help highlighting characteristic properties of the dynamics. With these conditions, the values of the $\tilde{\mathscr{H}}_{Att}(q_{30}, q_{40}, q_{50})$ at the equilibria, $\tilde{\mathscr{H}}_{Att\ Eq.i}$ with $i = 1, .., 6$, are shown in fig. 2.

To provide a description of $\tilde{\mathscr{H}}_{Att}(q_{30}, q_{40}, q_{50})$ over the three-dimensional domain, a sequence of iso-energy surfaces are shown in fig. 3. In particular, here only the energy levels associated with the equilibria, $\tilde{\mathscr{H}}_{Att\ Eq.i}$, have been plotted. In figure 3, the value of $\tilde{\mathscr{H}}_{Att}(q_{30}, q_{40}, q_{50})$ at the point determines the colour of the point itself. As the value increases from the minimum value to the maximum, the colour varies from dark blue to bright red, as it can be seen in the colour bars. The Hamiltonian map shows graphically the position of the equilibria, as identified in the previous section.

| Variable | Measure | Dimension |
|---|---|---|
| Total Body Length $l_i$ | 50 | cm |
| $\lvert d_i \rvert$ | 25 | cm |
| $m_i$ | 1.5 | $kg$ |
| $\mathbf{I}_i = \frac{1}{12} m_i l_i^2$ | 0.0078 | $kg\ m^2$ |

1: Data used for evaluating $\tilde{\mathscr{H}}_{Att}(q_{30}, q_{40}, q_{50})$. Bodies are considered orbiting around the Earth on a nominal orbit circular at an altitude of 300km above the surface.

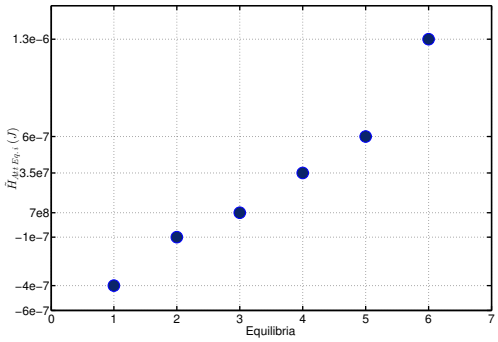


2: $\tilde{\mathscr{H}}_{Att}$ at the equilibria

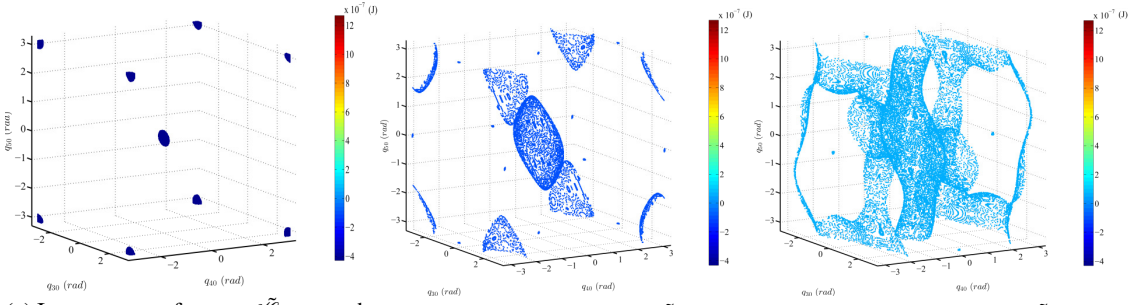

(a) Iso-energy surfaces at $\tilde{\mathscr{H}}_{Att\ Eq.1}$, the lowest value of $\tilde{\mathscr{H}}_{Att}$

(b) Iso-energy surfaces at $\tilde{\mathscr{H}}_{Att\ Eq.2}$

(c) Iso-energy surfaces at $\tilde{\mathscr{H}}_{Att\ Eq.3}$

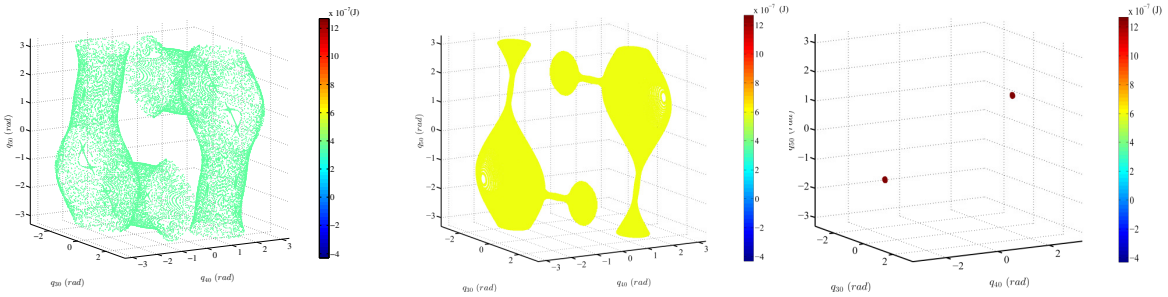

(d) Iso-energy surfaces at $\tilde{\mathscr{H}}_{Att\ Eq.4}$

(e) Iso-energy surfaces at $\tilde{\mathscr{H}}_{Att\ Eq.5}$

(f) Iso-energy surfaces at $\tilde{\mathscr{H}}_{Att\ Eq.6}$

3: Illustration of $\tilde{\mathscr{H}}_{Att}(q_{30}, q_{40}, q_{50})$ over its three-dimensional domain through a series of iso-energy surfaces. The elements of each manifold have the same value of $\tilde{\mathscr{H}}_{Att}$

Moreover, the stable equilibria are shown by small and isolated ellipsoids of low-energy colour. These surfaces are surrounded by higher energy manifolds which confine the motion on the equilibrium itself. On the contrary, unstable equilibria can be recognised as they are part of large manifolds which are surrounded by lower energy surfaces. A motion starting in the neighborhoods of these points can evolve on a large part of the domain or even in the whole domain. Finally, the map gives a description of the distribution of $\tilde{\mathscr{H}}_{Att}$ in all the attitude angles'domain, revealing a very complex structure underlying the dynamics od the problem. Equilibria are surrounded by ellipsoidal surfaces and some of them are connected by a "pipe-like" structure. These connections between equilibria can potentially be

used in the manoeuvre design by exploiting the system's natural motions for reconfigurations manoeuvres. It is worth noting the importance of the role of the physical parameters which might be used to introduce in the dynamics new connections between equilibria or "close" existing connections.

## SYSTEM BEHAVIOUR FAR FROM EQUILIBRIA

In order to provide a global description of the system behaviour, different representations of the dynamics will be shown using various analysis tools. The dynamic equations (11) are integrated and the trajectories analysed. Inspired by common techniques of integration using symplectic integrators, Hamiltonian and total angular momentum are introduced in the differential equations set in order to keep control of the numerical errors and to drive the accuracy of the integration always below a maximum relative error of an order of $o(10^{-13})$ on the initial values of the conserved quantities[2]. Conditions in table 1 are used in the following sessions.

### Phase Plots and Poincaré sections

Phase plots capture and show three different kinds of behaviours. Figure 4 shows projections of the trajectories of the system in the $\{q_4, q_5\}$, $\{q_4, \dot{q}_4\}$ and $\{q_5, \dot{q}_5\}$ planes. These projections are supported by the relative Poincaré sections. Poincaré sections are a standard technique to inspect complex systems. These are projections of phase spaces where a snap shot is taken whenever the trajectory intersects a prescribed plane in the phase space. Consequently, the Poincaré mapping[3] is a collection of points sampled in a regular way from the phase portraits. For this problem Poincaré sections are constructed sampling the state of the system when the following condition is verified: $\{\theta_1 = 0, \omega_1 \geq 0\}$. Here, the sections are provided in the same planes of phase plots[4].

In figure 4a a fully regular behaviour is observed[5]. The motion is periodic and its projections evolve over a line in the plane $\{q_4, q_5\}$ and over circles (clockwise) in the planes$\{q_4, \dot{q}_4\}$ and $\{q_5, \dot{q}_5\}$. Trajectories topologically equivalent to the one shown here have been observed for initial conditions in a relatively small[6] neighborhood of the stable equilibrium point.

Figure 4b shows a regular behaviour which is identified as "quasi-periodic" as it evolves in a bounded region on almost periodic trajectories without ever exactly coming back on themselves. In the Poincaré sections, the system's natural evolution is completely described by a set of points which appears to be aligned on a closed curve, even though not totally drawn. This feature is typical of quasi-periodic motions, for instance, see the Hénon-Heiles Poincaré section for $e = 0.08333$ in [23].

Finally, in figure 4c any sort of regularity disappears and the points cover an apparently random shaped area rather than being ordered along a curve. This kind of behaviour can be recognised in the Poincaré sections of many systems as the double pendulum, the three body system or again in the Hénon-Heiles equations for $e = 0.12500$, see [23].

### Poincaré Map

A Poincaré map is constructed collecting all the Poincaré sections generated from initial conditions which have $\tilde{\mathscr{H}}_{Att} = -3.96 \times 10^{-7}$ $J$. This energy state is chosen as it shows a wide range of different behaviours. Fig. 5a shows, which initial conditions belong to the indicated energy.

Each initial condition shown in fig.5a has been integrated and the trajectory analysed. The resulting Poincaré map is shown from three different projections in fig. 5.

Chaotic motion can be seen where the region is dense on the set, as shown in figures 5b, 5c and 5d. Invariant tori can be recognised in the regions at the center-bottom of 5b, the center of 5c and in center-top of 5d. In these areas,

---

[2] This solution has been preferred to the reduction of the system introducing into the equations the conserved quantities, in order to effectively have way of monitoring the magnitude order of the error.

[3] Also referred as a stroboscopic technique

[4] For further details on Poincaré maps, see [21] or [22].

[5] It should be noted that no dissipative forces have been included in the model.

[6] Note the magnitude orders of the x and y axis scales in fig.4a are particularly small.

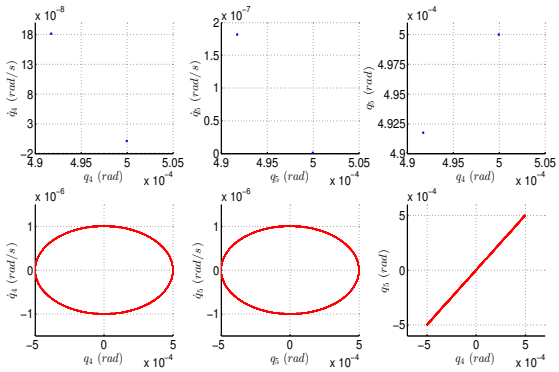

(a) Example of periodic behaviour of the system

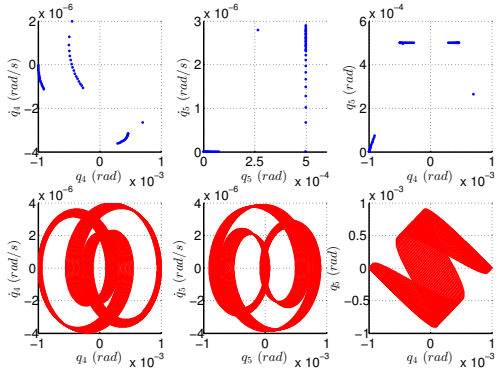

(b) Example of quasi-periodic behaviour of the system

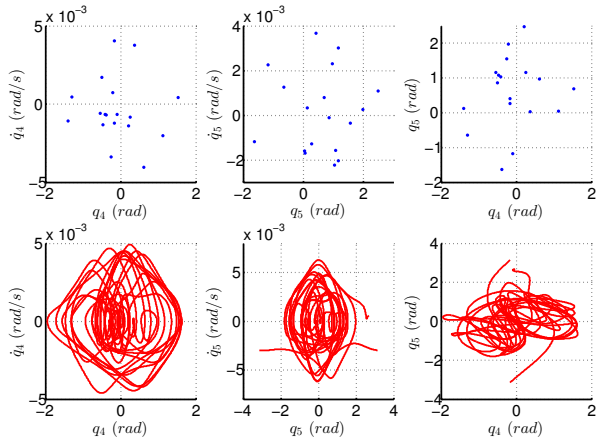

(c) Example of periodic behaviour of the system

4: Illustration of three different behaviours of the system using phase plots and Poincaré sections.

ordered sequences of concentric discontinuous lines in a layout typical of quasi-periodic motions can be found. This kind of structure clearly suggests the presence of motions developing into invariant tori. Furthermore, the boundary between different qualitative behaviours is fuzzy. There are some particular cases where the quasi-periodicity is weak and the motion can be classified as either quasi-periodic or chaotic.

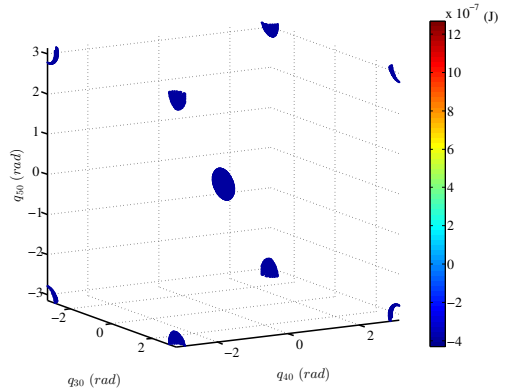


(a) Iso-energy surfaces at $\tilde{\mathscr{H}}_{Att\ Eq.0}$

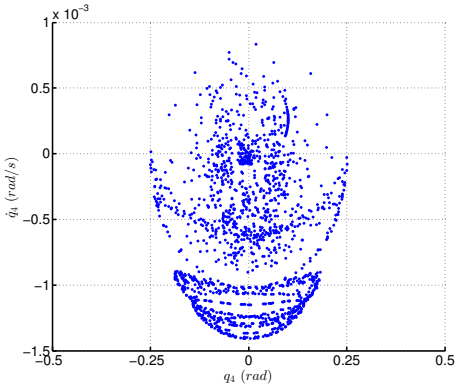


(b) Poincaré Map from $\tilde{\mathscr{H}}_{Att\ Eq.0}$ in the plane $(q_4, \dot{q}_4)$

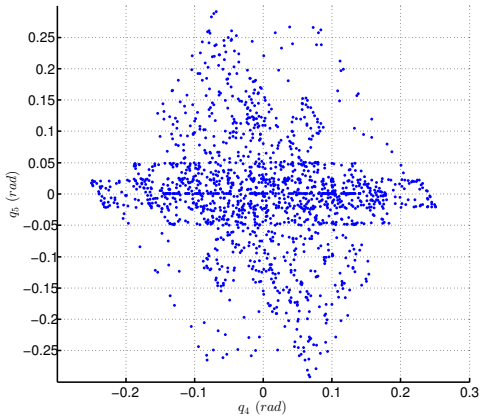


(c) Poincaré Map from $\tilde{\mathscr{H}}_{Att\ Eq.0}$ in the plane $(q_4, q_5)$

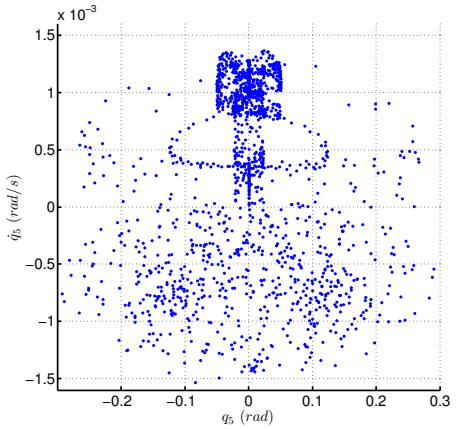


(d) Poincaré Map from $\tilde{\mathscr{H}}_{Att\ Eq.0}$ in the plane $(q_5, \dot{q}_5)$

5: A Poincaré Map of the problem

## CONCLUSIONS

A three finite-shape rigid-body system has been studied. The problem is restricted to the planar case and under the effect of an ideal gravitational field only. An Hamiltonian approach has been used to highlight conserved quantities of the problem and derive the dynamics. With the introduction of a negligible approximation error the orbital dynamics is taken as uncoupled from the attitude dynamics and the analysis of the problem restricted to the attitude dynamics behaviour only. This reveals six classes of relative equilibria. For every class each body is either aligned with the $X|_{ORF}$ or with the $Y|_{ORF}$, that is, parallel or perpendicular to the position vector of the overall center of mass with respect to the main inertial reference frame. A numerical investigation of the problem in the case of three equal bodies has been undertaken. First, the Hamiltonian has been studied graphically revealing a very complex structure underlying the dynamics. Connections between equilibria are observed. The analysis of the behaviour far from the equilibria has been undertaken using phase plots and Poincaré sections. Three different kinds of motions have been found: periodic, quasi-periodic and chaotic. Fully regular motions are observed only in a relatively small neighborhood of the stable equilibria. A Poincaré map for a given energy level of the initial conditions is provided. The map shows the presence of invariant tori as well as chaotic manifolds. In conclusion, the three-body-problem shows very complex dynamics

mostly driven by a chaotic behaviour with a number of 42 equilibria divided in 6 different classes. The presence of many connections between equilibria is identified as a potential element to design large reconfiguration manoeuvres using natural motions. Moreover, like the two-body problem, the choice of parameters may condition the stability of some of the equilibria and has been identified as a critical design factor. Future works will address the stability analysis of the equilibria as well as bifurcation studies of the system's dynamics based on the variation of the system's parameters.

## REFERENCES


1. NASA, On−orbit satellite servicing study, project report, Tech. rep., National Aeronautics and Space Administration Goddard Space Flight Center (2010), in publication.
2. C. Bonnal, J.-M. Ruault, and M.-C. Desjean, *Acta Astronautica, Active debris removal: Recent progress and current trends* **85**, 51 – 60 (2013).
3. D. Reintsema, J. Thaeter, A. Rathke, W. Naumann, P. Rank, and J. Sommer, "DEOS The German Robotics Approach to Secure and De−Orbit Malfunctioned Satellites from Low Earth Orbits," in *Proceeding of the Robotics and Automation in Space (i−SAIRAS)*, Sapporo, Japan, 2010.
4. T. Wolf, D. Reintsema, B. Sommer, P. Rank, and J. Sommer, "Mission DEOS Proofing the Capabilities of German's Space Robotic Technologies," in *Proceeding of the International Symposium on Artificial Intelligence, Robotics and Automation in Space i−SAIRAS*, 2012.
5. A. Ogilvie, and et al., "Autonomous satellite servicing using the orbital express demonstration manipulator system," in *Proc. of the 9th International Symposium on Artificial Intelligence, Robotics and Automation in Space (i−SAIRAS'08)*, 2008.
6. R. B. Friend, "Orbital Express program summary and mission overview," in *Proc. SPIE 6958, Sensors and Systems for Space Applications II*, Conference Volume 6958, April 15, 2008.
7. A. A. Shabana, *Dynamics of Multibody Systems, third edition*, Cambridge, 2005.
8. S. Dubowsky, and E. Papadopoulos, *IEEE Transactions on Robotics and Automation* **9** (1993).
9. Z. Vafa, and S. Dubowsky, *The International Journal of Robotics Research* **9** (1990).
10. E. Papadopoulos, *On the Dynamics and Control of Space Manipulators*, Ph.D. thesis, Department of Mechanical Engineering, Massachussetts Intitute of Technology (1990).
11. W. S. Koon, M. W. Lo, J. E. Marsden, and S. D. Ross, *Dynamical Systems, the Three-Body Problem and Space Mission Design*, CalTech, 2011.
12. C. Maclean, D. Pagnozzi, and J. Biggs, *IEEE Transactions on Aerospace and Electronic Systems* (2014), , ISSN 0018-9251 (In Press).
13. D. Pagnozzi, C. Maclean, and J. D. Biggs, "A new approach to the solution of free rigid body motion for attitude maneuvers," in *Proceeding of the European Control Conference 2013 (ECC13)*, IEEE Xplore, Zurich, Switzerland, 2013.
14. A. Sanyal, and A. Bloch, "Two connected bodies in a central gravitational field," in *Proceeding of the IEEE Conference on Decision and Control. CDC. 43rd*, 2004, p. 3968.
15. N. Sreenath, Y. Oh, P. Krishnaprasad, and J. Marsden, *Dynamics and Stability of Systems* **3** (1998).
16. A. Sanyal, A. Bloch, and N. H. McClamroch, *Journal of Dynamicsal Sytems* **19**, 303–343 (2004).
17. P. Santini, and P. Gasbarri, *Acta Astronautica* **64**, 1224 (2009).
18. O. I. Bogoyavlenskil, *Russian Acad. Sci. Izv. Math.* **41** (1993), http://iopscience.iop.org/1468-4810/41/3/A01.
19. P. Santini, and P. Gasbarri, *Acta Astronautica* **54**, 1 (2003).
20. D. Pagnozzi, and J. D. Biggs, "Lyapunov Characteristic Exponent Maps for Multi-Body Space Systems Analysis," in *Proceeding of the AIAA SciTech 2014 conference*, American Institute of Aeronautics and Astronautics, National Harbor, Maryland, USA, 2014.
21. J. Thompson, and H. Stewart, *Nonlinear Dynamics and Chaos*, John Wiley and Sons, 1986.
22. R. C. Hilborn, *Chaos and nonlinear dynamics : an introduction for scientists and engineers*, New York, Oxford University Press, 1994.
23. M. Hénon, and C. Heiles, *The Astronomical Journal* **69** (1964).